Joint Estimation of Vessel Position and Mooring Stiffness during Offshore Crane Operations

Jun Ye, Milinko Godjevac, Simone Baldi, and Hans Hopman

***Abstract*—Offshore heavy lift vessels are designed for transporting, installing and removing offshore facilities. Previous studies have shown that the time-varying forces acting on the main crane may result in an unstable Dynamic Positioning (DP) control system, which adversely affects the safety of the heavy lifting operation. Solutions based on force feedforward control thus has been proposed, i.e., the low-frequency horizontal component of the crane force is forwarded to the DP controller or observer. Accurate estimation of the horizontal component of the crane force is essential for the feedforward solution, but it is extremely difficult to obtain it from a measurement due to its time-varying nature and the non-linear system dynamics stemming from the ship-environment interaction. Therefore, in this work, we focus on the estimation of the low-frequency crane force in the horizontal direction during loading and offloading stages of a heavy lift operation in various environmental conditions. To achieve this goal, a novel time-varying mooring stiffness term is introduced, which is included in the nonlinear passive observer of the vessel and used in a joint parameter-state estimator to estimate the horizontal crane force and vessel states. Afterward, simulations are performed to test the estimator in various environmental and loading conditions. The results indicate that an accurate estimation of the low-frequency horizontal component of the crane force can be achieved by measuring the position of the ship and the tension in the wires even in the presence of large parameter uncertainty.**

***Index terms*—** Heavy Lift Construction; Offshore Mooring System; Joint Parameter-State Estimation

I. INTRODUCTION

Heavy lift vessels play an essential role in the installation and removal of oil platforms and other offshore structures since the mid-20th century [1, 2]. The interest in the study of offshore crane vessels was shown in the late 20th century: most of the early studies focused on the dynamics of the crane vessel in pitch [3, 4] and the interaction between the crane dynamics and ship motions [5–7].

During a typical offshore construction assignment with heavy lift vessels, there are three working modes: a free hanging mode, a lifting or offloading mode (mooring mode), and a mode without the crane load. When the heavy lift vessel works in the mooring mode (see Fig. 1), the vessel needs to stay in the position while the crane wires are attached to a platform until the work is done, and DP systems are widely applied for offshore positioning during such construction works.

J. Ye, M. Godjevac and Hans Hopman are with the Department of Maritime & Transport Technology, Delft University of Technology, Delft, 2628CD, the Netherlands e-mail of corresponding author: j.ye-1@tudelft.nl.

S. Baldi is with Delft Center for System and Control, Delft University of Technology.

This work is financially supported by the program of China Scholarships Council (CSC) with project No. 20167720003.

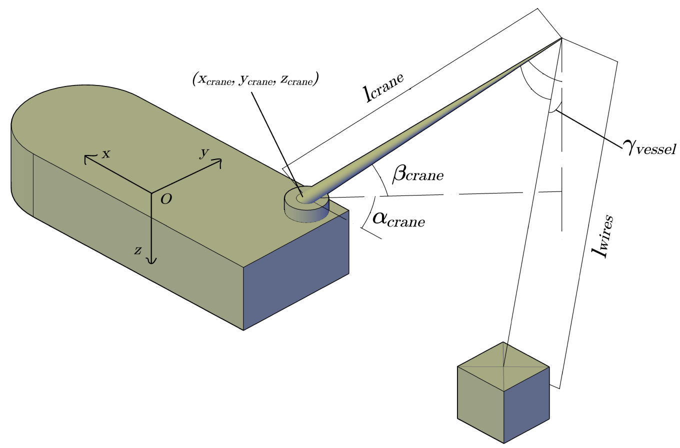

Fig. 1. Crane Vessel Moored to the Platform

However, a study from Flint and Stephens showed that a combination of the crane force and wrongly tuned controller gains of the DP system could lead to instability of the vessel position during mooring stage due to the added stiffness from the crane wires [8]. A more detailed case study on DP controlled offshore heavy lift operations could be found in the study of Vorhölter with simulations in time domain for three different lifting vessels [9]. This study has shown that already with a small load mass, e.g., 2% of the vessel displacement, the impact of the crane force on the motion behavior of the vessel is significant.

Therefore, many studies have been carried out on the subject of control systems for offshore cranes and offshore heavy lift vessels to solve this stability problem during mooring mode and to stabilize the crane load when the load is free-hanging. Among these studies, some control methods have been developed to stabilize the sway angle and load position of the overhead free-hanging crane load [10–18]. In these control methods, sway angle or load position was measured by virtual sensors while the mooring mode was not investigated. For the offshore mooring mode, solutions such as feedforward to the estimator and robust controller were proposed to solve the stability problem [19, 20]. According to the simulation results from these studies, the feedforward solutions provided satisfying results, but the estimation of the feedforward horizontal component of the crane force or the sway angle of the load was not mentioned.

Similar problems exist in the field of the positioning of icebreakers under unknown ice load. During the position and motion control of the icebreaker, the unknown ice load could be estimated as part of slowly varying external load [21–23]. However, in the mooring mode of the heavy lift operations, the low-frequency part of external excitation is with a much smaller period, which makes it difficult to distinguish the crane load from the slowly-varying environmental load. Therefore, a reaction force observer was designed to estimate the horizontal force and the sway angle in one DOF [11]. Due to the limitation of the DOFs and the absence of external disturbances, these methods could not be directly applied in a DP controlled heavy lift vessel during mooring mode.

In this paper, the low-frequency crane force under heavy lift mooring mode is estimated using a joint position-force nonlinear estimator. To facilitate the estimation, we introduce a stiffness parameter that captures the effect of the nonlinear and time-varying dynamics. First, a model of the vessel with a crane at the aft end is made to simulate the 6 DOFs behavior of the vessel. This model includes a hydraulic winch with the crane, vessel motion, environmental loads, and actuators. The hydraulic winch controls the force in the crane wires, and the environmental load consists of three parts: wave, wind, and current. Both the vessel and the crane are modeled as rigid bodies. Three bow thrusters and two propellers are designed as the actuators. The horizontal component of the crane force is estimated by introducing a new parameter, the mooring stiffness term. A nonlinear passive observer is made to estimate the position of the vessel and the mooring stiffness in real time to find the horizontal force and moment on the vessel caused by the crane wires. In the end, different simulations are made to test the robustness and stability of the designed observer in combination with the simulated vessel behavior.

The main contribution of this paper is the joint estimation of the vessel position and the low-frequency horizontal crane force with limited measurements during the mooring mode. There are several innovations in this work: (1) The estimation is based on standard and inexpensive measurements, which include vessel position and absolute crane force. In particular, as opposed to state of the art, the measurements of the vessel velocity and the crane wires' sway angle are not required; (2) Simulations are made with a vessel model with 6 DOFs, whereas most previous works on the subject only consider roll or pitch dynamics; (3) The method is simulated under several environmental conditions and practical assumptions such as time delay in the propulsion system and noise in the measured data.

The rest of the paper is organized as follows: In Section II, the simulation model of heavy lift mooring mode is provided. In Section III, the joint observer is designed. In Section IV, the simulation settings for different environmental conditions are explained, and simulation results are shown and analyzed. Conclusions are drawn in Section V, and the paper ends with recommendations for future work.

II. Simulation Model

A simulation model of the vessel is generated by WAMIT and is based on the S-175 model from MSS toolbox [25].

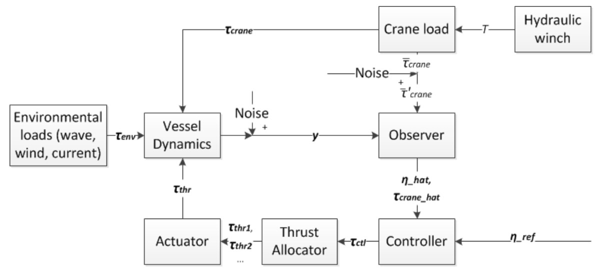

Fig. 2. Overall Simulation Model for the Moored Heavy Lift Vessel

The overall model with the control system is shown in Fig. 2. The model includes environmental loads, vessel dynamics, hydraulic crane, controller and thrust allocator, which are described in detail in this section.

The following standard assumptions, all mutated from [26], are made for the simulation model and the designed observer:

Assumption 1: The vessel is symmetrical in starboard and port. The hydrodynamic added mass terms are fixed. This assumption holds for low-speed applications.

Assumption 2:The bias model and the wave model are driven by zero-mean Gaussian noise. This assumption is made to simplify the modelling of the wave and current.

Assumption 3: The offset of the vessel in surge, sway and yaw is small as compared to the size of the ship. This is reasonable, because nowadays vessels are controlled by DP systems which keep the offsets within 5 meters.

Assumption 4: Wave-induced yaw disturbance is neglectable in rotation matrix.

A. Vessel Dynamics

In the following, $\boldsymbol{I}$ stands for identity matrix, $\mathbf{0}$ stands for null matrix, and $\boldsymbol{R}$ stands for rotation matrix from body-fixed coordinate system to earth-fixed coordinate system.

The simulation model in 6 DOFs for the vessel dynamics including ocean current can be expressed as the following[26]:

$$\begin{aligned}(\boldsymbol{M}_{RB}+\boldsymbol{M}_A)\dot{\boldsymbol{v}}+\boldsymbol{C}(\boldsymbol{v}_r)\boldsymbol{v}_r+\boldsymbol{D}_s\boldsymbol{v}_r\\ =\boldsymbol{\tau}_{wind}+\boldsymbol{\tau}_{wave}+\boldsymbol{\tau}_{thr}+\boldsymbol{\tau}_{crane}\end{aligned} \tag{1}$$

$$\dot{\boldsymbol{\eta}}=\boldsymbol{R}(\phi,\theta,\psi)\boldsymbol{v} \tag{2}$$

where (1) holds under the assumption that the vessel is moving with low velocity and low acceleration, $\boldsymbol{\eta}=[x,y,z,\phi,\theta,\psi]^\top$ is the position of the vessel in earth-fixed frame, $\boldsymbol{v}=[u,v,w,p,q,r]^\top$ is the velocity of the vessel in body frame, $\boldsymbol{v}_r=\boldsymbol{v}-\boldsymbol{v}_c$ is the relative velocity of the vessel with respect to the current velocity, $\boldsymbol{v}_c=[u_c,v_c,w_c,0,0,0]^\top$ is the current velocity, $\boldsymbol{\tau}_{wind}$ is the wind load, $\boldsymbol{\tau}_{wave}$ is the wave load, $\boldsymbol{\tau}_{thr}$ is the thrust force, and $\boldsymbol{\tau}_{crane}$ is the external force from the crane wires.

The inertia matrix $\boldsymbol{M}_{RB}\in\mathbb{R}^{6\times6}$ is defined as:

$$\boldsymbol{M}_{RB}=\begin{bmatrix} m\boldsymbol{I}_{3\times3} & -m\boldsymbol{S}(\boldsymbol{r}_g^b)\\ m\boldsymbol{S}(\boldsymbol{r}_g^b) & \boldsymbol{J}_v\end{bmatrix} \tag{3}$$

where m is the weight of the vessel, $\boldsymbol{J}_v$ is the inertia moment matrix in roll pitch and yaw, $\boldsymbol{r}_g^b$ is the vector from Center of Origin to Center of Gravity expressed in body frame, and the cross-product is defined as $\boldsymbol{a} \times \boldsymbol{b} = \boldsymbol{S}(\boldsymbol{a})\boldsymbol{b}$.

In (1), $\boldsymbol{M}_A \in \mathbb{R}^{6\times6}$ is the added mass and added inertia matrix of the vessel. For a vessel which is symmetric on port-starboard, the added mass and added inertia matrix can be expressed as:

$$\boldsymbol{M}_A = \begin{bmatrix} m_{11} & 0 & m_{13} & 0 & m_{15} & 0 \\ 0 & m_{22} & 0 & m_{24} & 0 & m_{26} \\ m_{31} & 0 & m_{33} & 0 & m_{35} & 0 \\ 0 & m_{42} & 0 & m_{44} & 0 & m_{46} \\ m_{51} & 0 & m_{53} & 0 & m_{55} & 0 \\ 0 & m_{62} & 0 & m_{64} & 0 & m_{66} \end{bmatrix} \tag{4}$$

where m_{ij} can be expressed as: $m_{ij} = \rho \oint_S \varphi_i \frac{\partial \varphi_j}{\partial n} dS$, where ρ is the density of water, S is the wetted ship area, φ_i is the flow potential when the vessel is moving in ith direction.

In addition, $\boldsymbol{C} \in \mathbb{R}^{6\times6}$ is the Coriolis-centripetal matrix, $\boldsymbol{D}_s \in \mathbb{R}^{6\times6}$ is the damping matrix of the vessel, and $\boldsymbol{R}(\phi,\theta,\psi) \in \mathbb{R}^{6\times6}$ is the rotation matrix in 6 DOFs. The calculation of $\boldsymbol{R}(\phi,\theta,\psi)$, $\boldsymbol{C}$ and $\boldsymbol{D}_s$ can be found in the book by Fossen [26].

B. Environmental Loads

The environmental loads can be seen as the combination of wind load and wave load.

Wind causes additional air pressure to the surface of the vessel. Wind load is related to the surface of the vessel, wind velocity and attack angle of the wind. For a vessel in DP control mode with zero speed over ground, the wind load can be defined as:

$$\boldsymbol{\tau}_{wind} = \begin{bmatrix} \frac{1}{2}\rho_a V_w^2 C_X(\gamma_w) A_{Fw} \\ \frac{1}{2}\rho_a V_w^2 C_Y(\gamma_w) A_{Lw} \\ \frac{1}{2}\rho_a V_w^2 C_Z(\gamma_w) A_{Fw} \\ \frac{1}{2}\rho_a V_w^2 C_K(\gamma_w) A_{Lw} H_{Lw} \\ \frac{1}{2}\rho_a V_w^2 C_M(\gamma_w) A_{Fw} H_{Fw} \\ \frac{1}{2}\rho_a V_w^2 C_N(\gamma_w) A_{Lw} L_{oa} \end{bmatrix} \tag{5}$$

where ρ_a is air density, V_w is wind speed, which is modeled as a combination of slow-varying wind and wind gust, C_X, C_Y, C_Z, C_K, C_M, and C_N are nondimensional coefficients related to the attack angle of the wind. A_{Fw} and A_{Lw} are the frontal and lateral project areas above the waterline, while H_{Fw} and H_{Lw} are the centroids of the two areas, and γ_w is the attack angle of the wind. The wind angle is slowly varying around the mean wind angle. An example of wind load on the vessel during DP operation is shown in Fig. 4 for the surge, sway and yaw directions with the mean wind speed of 2.5 m/s and a nominal wind angle of 210°.

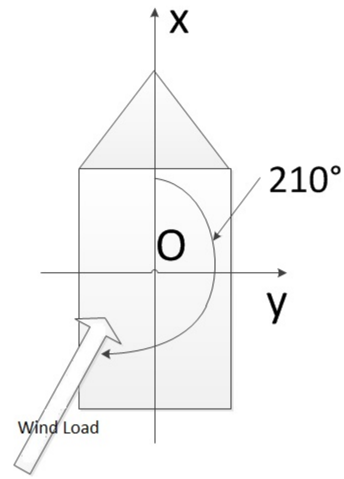

Fig. 3. Illustration of Environmental Load

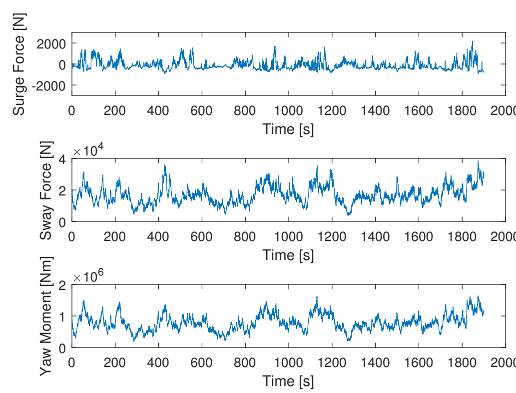

Fig. 4. Wind Load

The wave load consists of a first order wave load and a second order slowly varying wave load.

$$\boldsymbol{\tau}_{wave} = \boldsymbol{\tau}_{wave1} + \boldsymbol{\tau}_{wave2} \tag{6}$$

The second order wave load $\boldsymbol{\tau}_{wave2}$ is modeled as a mean wave drift load without an oscillatory component. First order wave induced load $\boldsymbol{\tau}_{wave1}$ is a zero mean oscillation load. Where first order and second order wave loads can be found in [26]. Examples of the first order and second order wave loads with a significant wave height of 0.5m and a peak frequency of 0.8 rad/s with Jonswap spectrum are shown in Fig. 5 and Fig. 6.

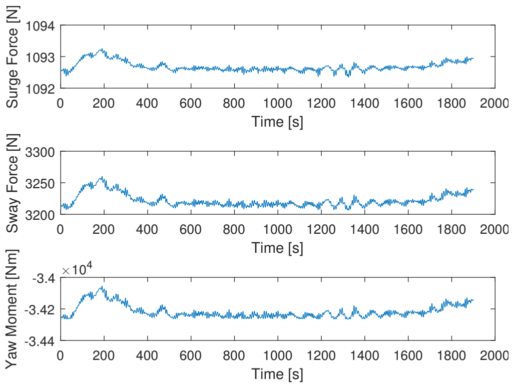

Fig. 5. Second Order Wave Load

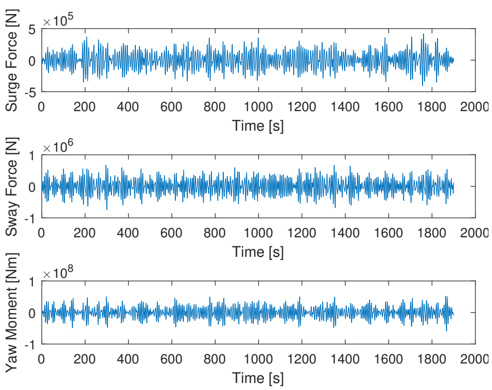

Fig. 6. First Order Wave Load

C. Hydraulic Crane

The crane wires are simplified as a spring and a damper:

$$F_{hoist} = k_{wires}(l_{wires} - l_{ini}) + D\frac{d(l_{wires} - l_{ini})}{dt} \tag{7}$$

where F_{hoist} is the force in the crane wires, k_{wires} is the stiffness of the crane wires, D is the damping term of the wires, l_{wires} and l_{ini} are the length and initial length of the crane wires. During the simulation, l_{ini} is changing to adjust the output torque from the hydraulic motor.

The crane winch is actuated by a hydraulic motor. The output torque of the hydraulic motor is[27]:

$$T = \frac{\eta_{hyd} Q \Delta p}{2\pi} \tag{8}$$

$$\bar{\tau}_{crane} = \frac{T}{r} \tag{9}$$

where T is the torque output of the hydraulic motor, Q is the inlet flow rate per revolution, Δp is the pressure difference between the inlet flow and the outlet flow, η_{hyd} is the efficiency of the motor, r is the radius if the drum that the cable is wound on. During the simulation, the crane force is determined by the hydraulic motor. The hydraulic motor is controlled by a PI controller, with the control gains K_{hp} and K_{hi}. It is assumed that the pressure difference of the motor is constant in the simulation and only the inlet flow rate is changing to give desired crane force output. Thus the PI controller in the hydraulic crane is:

$$Q = K_{hp}\delta T + K_{hi}\int \delta T dt \tag{10}$$

where δT is the difference between the desired torque and the actual torque.

D. Propulsion System

In order to properly capture the dynamics of the propulsion system we used a mean-value first principle modelling approach to model the engine-propeller interaction.For more details on the modeling approach for each of the subcomponents, please refer to the paper from Godjevac [28]. The propulsion model in this work has been validated in [29].

The diesel engine is modeled as a four-stroke engine with six cylinders:

$$M_b = \frac{6\eta_e m_f k_{LHV} n_{eng}}{2\pi n_{eng}} \tag{11}$$

where M_b is the output torque, η_e is the efficiency, m_f is the fuel injection in gramme, k_{LHV} is the ratio of energy and mass of the fuel, and n_{eng} is the engine speed in rotation per second.

The thrust force for each thruster i is:

$$\begin{aligned} \bar{\tau}_{thri} &= \rho n^2 D^4 K_t && (12)\\ &= \rho n^2 D^4 (K_{ta} J + K_{tb}) && (13) \end{aligned}$$

where ρ is the water density, n is the rate of revolution, D is the diameter of the propeller, K_{ta} and K_{tb} are two constant parameters, J is a nondimentional expression of the propeller which equals to $\frac{V_A}{nD}$, and V_A is the arriving water velocity.

Similarly, the propeller torque is:

$$\begin{aligned} M_p &= \rho n^2 D^5 K_q && (14)\\ &= \rho n^2 D^4 (K_{qa} J + K_{qb}) && (15) \end{aligned}$$

A shaft is connecting the diesel engine and the propeller.

$$\begin{aligned} n_p &= \frac{n_e}{i_{gb}} && (16)\\ &= \int \frac{M_b \eta_{trm} i_{gb} - M_p}{2\pi I_{tot}} dt && (17) \end{aligned}$$

where i_{gb} is the gearbox ratio, η_{trm} is the transmission efficiency, and I_{tot} is the total mass of inertia of the propulsion system.

For the overall thrust force on the vessel,

$$\boldsymbol{\tau}_{thr} = \sum \boldsymbol{\tau}_{thri} \tag{18}$$

where the summation is to be intended as vector summation.

E. Controller and Thrust Allocator

A PID controller is adopted in the simulations as DP controller with the control force:

$$\boldsymbol{\tau}_{ctl} = \boldsymbol{K}_p\boldsymbol{e} + \boldsymbol{K}_i\int \boldsymbol{e}dt + \boldsymbol{K}_d\dot{\boldsymbol{e}} \tag{19}$$

Where $\boldsymbol{e} = \hat{\boldsymbol{\eta}} - \boldsymbol{\eta}_{ref}$ is the error between estimated position $\hat{\boldsymbol{\eta}}$ and desired position $\boldsymbol{\eta}_{ref}$.

A simple thrust allocator is designed using one time-invariant matrix. The thrust forces in each thruster can be calculated using the following formula:

$$\begin{bmatrix} \bar{\tau}_{thr1} \\ \bar{\tau}_{thr2} \\ \bar{\tau}_{thr3} \\ \dots \end{bmatrix} = \boldsymbol{B}_{TA}\boldsymbol{\tau}_{ctl} \tag{20}$$

where $\boldsymbol{B}_{TA}$ is the time-invariant matrix of the thrust allocator.

The ballasting system on board is not modeled, thus the vessel would have a pitch angle when there's vertical crane load in the crane wires. The vessel's center of origin in Body frame would also change due to the pitch angle.

III. Observer Design

In this section, the designed observer for the vessel-crane moored system is provided. Two sets of measurements are required for the observer: vessel position $\boldsymbol{y}$ as a vector and the crane force $\bar{\tau}_{crane}$ as a scalar. Note that the goal of the observer is to estimate the low-frequency vessel movement in surge, sway and yaw, and the low-frequency horizontal crane force. This is because the DP system cannot cope with high-frequency variations.

A. Control Plant Model

The controlled system can be modeled as a second-order system. In the position control system, only the low frequency part, which contains the movement in surge, sway and yaw of the vessel movement, is controlled. Thus the 3 DOFs control plant model can be simplified as:

$$\dot{\boldsymbol{\xi}} = \boldsymbol{A}_w\boldsymbol{\xi} \tag{21}$$

$$\dot{\boldsymbol{\eta}} = \boldsymbol{R}(\psi)\boldsymbol{v} \tag{22}$$

$$\dot{\boldsymbol{b}} = -\boldsymbol{T}_b^{-1}\boldsymbol{b} + \boldsymbol{w}_b \tag{23}$$

$$\boldsymbol{M}\dot{\boldsymbol{v}} + \boldsymbol{D}\boldsymbol{v} = \boldsymbol{\tau}_{wind} + \boldsymbol{\tau}_{ctl} + \boldsymbol{\tau}_{crane} + \boldsymbol{R}^T(\psi)\boldsymbol{b} \tag{24}$$

$$\boldsymbol{y} = \boldsymbol{\eta} + \boldsymbol{C}_w\boldsymbol{\xi} + \boldsymbol{w}_1 \tag{25}$$

$$\bar{\tau}'_{crane} = \bar{\tau}_{crane} + w_2 \tag{26}$$

where $\boldsymbol{\xi}$ is the pertubation from first order wave load, $\boldsymbol{\eta}$ is the vessel's position in three DOFs in North-East-Down coordinate system, $\boldsymbol{v}$ is the velocity of the vessel in body frame, τ'_{crane} is the measured crane force in scalar, $\boldsymbol{b}$ is the bias term which includes the slowly varying external force, $\boldsymbol{w}_b$ is the Wiener process, and $\boldsymbol{w}_1$ and w_2 are the Gaussian white noise, $\boldsymbol{A}_w \in \mathbb{R}^{6\times6}$ and $\boldsymbol{C}_w \in \mathbb{R}^{3\times6}$ are two matrices describing the wave load, $\boldsymbol{R}(\psi) \in \mathbb{R}^{3\times3}$ is the transfer matrix from body to NED frame, $\boldsymbol{T}_b \in \mathbb{R}^{3\times3}$ is the time constant matrix for the bias, $\boldsymbol{M} \in \mathbb{R}^{3\times3}$ is the sum of rigid body mass matrix and added mass matrix of the vessel in 3 DOFs.

B. Mooring Stiffness

During moored dynamic positioning, there is additional stiffness added to the vessel because of the crane force. The vessel during mooring status can be seen as added with extra horizontal stiffness.

The damping term of the wires can be neglected comparing to the stiffness of the wires. The setpoint of the vessel position is chosen where the crane wires are vertical, and the horizontal crane force is $\mathbf{0}$. Assuming that the offset of the vessel comparing to the setpoint position is small, the moored crane force can be approximated as the influence of both the offset and a changing mooring stiffness.

$$F_{hoist} = k_{wires}(l_{wires} - l_{ini}) \tag{27}$$

Assuming that the roll and pitch angle are small and their influence on the crane force can be neglected, we have the following equations:

$$\sin\gamma_{vessel} = \frac{\sqrt{\Delta x^2 + \Delta y^2}}{l_{wires}} \tag{28}$$

$$F_{horizon} = F_{hoist}\sin\gamma_{vessel} \tag{29}$$

where Δx is the surge position of the vessel comparing to the nominal position. Δy is the sway position of the vessel comparing to the nominal sway position. Mooring stiffness $\boldsymbol{k}'$ is defined as the horizontal stiffness of the vessel added by the crane wires.

$$\boldsymbol{F}_{horizon} = \boldsymbol{k}'\boldsymbol{R}^T(\psi)\Delta\boldsymbol{\eta} \tag{30}$$

Where $\Delta\boldsymbol{\eta}$ is the position offset comparing to the nominal position, which is also the setpoint for the position in this case.

C. Estimated States and Parameters

During dynamic positioning, the vessel's position and velocity should be estimated as well as the horizontal force from the crane wires. In this section, a joint state-parameter estimator is made. The estimated parameters are the mooring stiffness from the crane force and the states to be estimated include the position and velocity of the vessel in surge, sway, and yaw.

For the crane force in the surge and sway direction, the mooring stiffness can be simplified when the offset of vessel position is small.

$$k_{surge} = k_{sway} = k_0 = \frac{F_{surge}}{\Delta x} = \frac{F_{horizon}}{\sqrt{\Delta x^2 + \Delta y^2}} \tag{31}$$

$$k_0 = F_{hoist} \frac{\sqrt{\Delta x^2 + \Delta y^2}}{l_{hoist}\sqrt{\Delta x^2 + \Delta y^2}} = \frac{F_{hoist}}{l_{ini} + \frac{F_{hoist}}{k_{wires}}} \tag{32}$$

Thus the horizontal mooring stiffness in surge direction can be approximated as:

$$k_0 \approx \frac{F_{hoist}}{l_0} \tag{33}$$

Where l_0 is the initial length of the crane wires at the beginning of the construction work.

If the coupling between sway force and yaw moment is taken into consideration, the approximated mooring stiffness matrix $\boldsymbol{k}'$ can be written as:

$$\boldsymbol{k}' = \begin{bmatrix} k_0 & 0 & 0 \\ 0 & k_0 & -R_{ct}k_0 \\ 0 & -R_{ct}k_0 & R_{ct}^2 k_0 \end{bmatrix} \tag{34}$$

Where R_{ct} is the length from Center of Gravity of the vessel to the crane tip in the horizontal plane.

D. Equations for Joint Parameter-State Nonlinear Passive Observer

The original nonlinear passive observer was introduced by Fossen [8]. The objective of the original observer is to generate low-frequency motion of the vessel in the horizontal plane, as well as to estimate the slowly varying biased term. In addition to this, we would also want to know the horizontal force of the crane wires and estimate the mooring stiffness in this work. In addition to the original nonlinear passive observer, an equation for the estimation of horizontal crane force is developed. The overall observer is illustrated in Fig. 7.

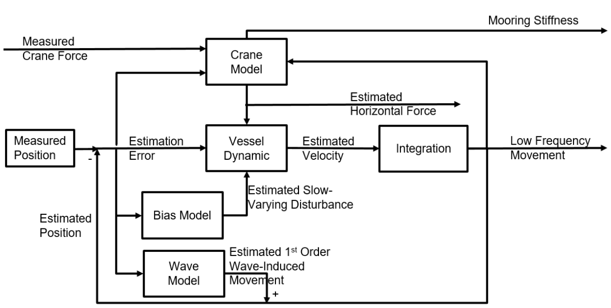

Fig. 7. Overall Illustration of the Observer

The equations of the observer are shown below:

$$\boldsymbol{M}\dot{\hat{\boldsymbol{v}}} = -\boldsymbol{D}\hat{\boldsymbol{v}} + \boldsymbol{R}^T(\psi)\hat{\boldsymbol{b}} + \boldsymbol{\tau}_{ctl} + \boldsymbol{R}^T(\psi)\boldsymbol{K}_4\tilde{\boldsymbol{y}} - \hat{\boldsymbol{\tau}}_{crane} \tag{35}$$

$$\hat{\boldsymbol{y}} = \hat{\boldsymbol{\eta}} + \boldsymbol{C}_w\hat{\boldsymbol{\xi}} \tag{36}$$

$$\dot{\hat{\boldsymbol{\eta}}} = \boldsymbol{R}\hat{\boldsymbol{v}} + \boldsymbol{K}_2\tilde{\boldsymbol{y}} \tag{37}$$

$$\dot{\hat{\boldsymbol{\xi}}} = \boldsymbol{A}_w\hat{\boldsymbol{\xi}} + \boldsymbol{K}_1\tilde{\boldsymbol{y}} \tag{38}$$

with the bias model:

$$\dot{\hat{\boldsymbol{b}}} = \boldsymbol{T}_b^{-1}\hat{\boldsymbol{b}} + \boldsymbol{K}_3\tilde{\boldsymbol{y}} \tag{39}$$

and the horizontal crane force model:

$$\hat{\boldsymbol{\tau}}_{crane} = \hat{\boldsymbol{k}}\boldsymbol{R}^T(\psi)(\hat{\boldsymbol{\eta}}' - \boldsymbol{\eta}_{ref}) \tag{40}$$

Equation (40) is the additional equation for the estimation of horizontal crane force. $\hat{\boldsymbol{\eta}}'$ in Equation (40) includes the influence from the pitch and roll angle. The equation for $\hat{\boldsymbol{\eta}}'$ is shown below:

$$\hat{\boldsymbol{\eta}}' = \hat{\boldsymbol{\eta}} + \boldsymbol{q}\begin{bmatrix} \sqrt{x_{ct}^2 + y_{ct}^2}\cos(\arctan|\frac{x_{ct}}{z_{ct}}| - \theta) - |x_{ct}| \\ |z_{ct}|\sin\phi \\ -\arcsin\frac{|z_{ct}|\sin\phi}{|x_{ct}|} \end{bmatrix} \tag{41}$$

Where $[x_{ct}, y_{ct}, z_{ct}]^\top$ is the position of cranetip in body frame, $\boldsymbol{q}$ is a tuning parameter, which is a diagnal matrix in this case.

The mooring stiffness is estimated by the equation below:

$$\hat{\boldsymbol{k}} = \boldsymbol{k}' + \boldsymbol{K}_5\tilde{\boldsymbol{y}} \tag{42}$$

If written in the state-space form, then

$$\dot{\hat{\boldsymbol{\eta}}}_0 = \boldsymbol{A}_0\hat{\boldsymbol{\eta}}_0 + \boldsymbol{B}_0\boldsymbol{R}\hat{\boldsymbol{v}} + \boldsymbol{K}\tilde{\boldsymbol{y}} \tag{43}$$

$$\hat{\boldsymbol{y}} = \boldsymbol{C}_0\hat{\boldsymbol{\eta}}_0 \tag{44}$$

where $\hat{\boldsymbol{\eta}}_0 = [\hat{\boldsymbol{\xi}}^\top, \hat{\boldsymbol{\eta}}^\top]^\top$

The errors are defined as $\tilde{\boldsymbol{\alpha}} = \boldsymbol{\alpha} - \hat{\boldsymbol{\alpha}}$, where $\boldsymbol{\alpha}$ stands for the real value in the system and $\hat{\boldsymbol{\alpha}}$ stands for the estimated value. Thus the error dynamics are shown as:

$$\boldsymbol{M}\dot{\tilde{\boldsymbol{v}}} = -\boldsymbol{D}\tilde{\boldsymbol{v}} + \boldsymbol{R}^T(\psi)\tilde{\boldsymbol{b}} - \boldsymbol{R}^T(\psi)\boldsymbol{K}_4\tilde{\boldsymbol{y}} - \tilde{\boldsymbol{F}}_c \tag{45}$$

$$\dot{\tilde{\boldsymbol{\eta}}}_0 = (\boldsymbol{A}_0 - \boldsymbol{K}\boldsymbol{C}_0)\tilde{\boldsymbol{\eta}}_0 + \boldsymbol{B}_0\boldsymbol{R}\tilde{\boldsymbol{v}} \tag{46}$$

$$\dot{\tilde{\boldsymbol{b}}} = \boldsymbol{T}_b^{-1}\tilde{\boldsymbol{b}} - \boldsymbol{K}_3\tilde{\boldsymbol{y}} \tag{47}$$

$$\tilde{\boldsymbol{\tau}}_{crane} = \tilde{\boldsymbol{k}}\boldsymbol{R}^T(\psi)(\hat{\boldsymbol{\eta}}' - \boldsymbol{\eta}_{ref}) \tag{48}$$

$$\tilde{\boldsymbol{k}} = -\boldsymbol{E}_t - F_{error}\boldsymbol{F}_0 + \boldsymbol{K}_5\tilde{\boldsymbol{y}} \tag{49}$$

where $\boldsymbol{E}_t \in \mathbb{R}^{3\times 3}$ is the time varying estimation error which is dependent on the offset of the vessel. F_{error} is the crane force measurement error. $\boldsymbol{F}_0 \in \mathbb{R}^{3\times 3}$ is a constant mapping matrix. The passivity and global stability of the original observer are proved by Fossen[30]. However, due to the coupling between the error dynamics in this observer design, it is difficult to prove stability in a mathematical way. Simulations in the next section show that the observer is stable and robust under several different simulation environments.

IV. Simulations

In this section, simulations are made to test the designed observer during mooring stage of the offshore heavy lift operations. The proposed observer is simulated with a variation of different parameters to test the performance of the observer as a function of environmental loads, loading and offloading rates, maximum crane load, measurement noise, and parameter uncertainty. Firstly the global settings of all simulations are introduced and afterward the result of each simulation is discussed. More detailed results in figures can be found in the appendix.

A. Simulation Settings

Simulations are made using a crane vessel which is 175m in length between perpendiculars with a draught of 7.5m and a breadth of 25.4m. The vessel has a mass of 24,609 tonnes. A crane with wires and a hydraulic winch is added to the vessel model. The propulsion system consists of two propellers and three tunnel thrusters. The crane parameters are chosen as:

$$[x_{crane}, y_{crane}, z_{crane}] = [-75, 0, -10] \tag{50}$$

$$[\alpha_{crane}, \beta_{crane}, l_{crane}] = [0, \frac{1}{3}\pi, 80] \tag{51}$$

$$l_{ini} = 70 \tag{52}$$

The Propulsion system of the vessel is set with three bow thrusters and two propellers as in Fig. 8. The propellers and the bow thrusters have a diameter of $3m$ and a relative rotative efficiency of 1.01. The nominal engine powers for the engines are $960kW$.

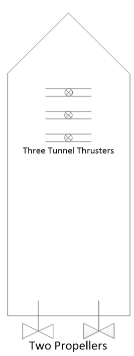

Fig. 8. Propulsion Setting

The positions of the three tunnel thrusters in body-fixd frame are chosen as $[70\ \ 0], [55\ \ 0], [40\ \ 0]$. The positions of the two propellers in body-fixd frame are chosen as $[-80\ \ -11], [-80\ \ 11]$. Accordingly, $\boldsymbol{b}_{TA}$ in (20) is:

$$\boldsymbol{B}_{TA} = \begin{bmatrix} 0.5 & 0 & 0 \\ 0.5 & 0 & 0 \\ 0 & -\frac{8}{3} & \frac{1}{30} \\ 0 & \frac{8}{3} & 0 \\ 0 & 1 & -\frac{1}{30} \end{bmatrix} \tag{53}$$

The PID gains in (20) are set as:

$$\boldsymbol{K}_p = \begin{bmatrix} 7000 & 0 & 0 \\ 0 & 200000 & 0 \\ 0 & 0 & 25000000 \end{bmatrix} \tag{54}$$

$$\boldsymbol{K}_i = \begin{bmatrix} 20 & 0 & 0 \\ 0 & 200 & 0 \\ 0 & 0 & 20000 \end{bmatrix} \tag{55}$$

$$\boldsymbol{K}_d = \begin{bmatrix} 500 & 0 & 0 \\ 0 & 500 & 0 \\ 0 & 0 & 0 \end{bmatrix} \tag{56}$$

The parameters of the observer are chosen as:

$$\boldsymbol{C}_w = \begin{bmatrix} \boldsymbol{0}_{3\times3} & \boldsymbol{I}_{3\times3} \end{bmatrix} \tag{57}$$

$$\boldsymbol{A}_w = \begin{bmatrix} \boldsymbol{0}_{3\times3} & \boldsymbol{I}_{3\times3} \\ -0.64\boldsymbol{I}_{3\times3} & -0.64\boldsymbol{I}_{3\times3} \end{bmatrix} \tag{58}$$

$$\boldsymbol{K}_1 = \begin{bmatrix} -1 & 0 & 0 \\ 0 & -1 & 0 \\ 0 & 0 & -1 \\ 0.64 & 0 & 0 \\ 0 & 0.64 & 0 \\ 0 & 0 & 0.64 \end{bmatrix} \tag{59}$$

$$\boldsymbol{K}_2 = \boldsymbol{I}_{3\times3} \tag{60}$$

$$\boldsymbol{K}_3 = \begin{bmatrix} 0.1 & 0 & 0 \\ 0 & 0.1 & 0 \\ 0 & 0 & 0.01 \end{bmatrix} \tag{61}$$

$$\boldsymbol{K}_4 = \begin{bmatrix} 1 & 0 & 0 \\ 0 & 1 & 0 \\ 0 & 0 & 0.1 \end{bmatrix} \tag{62}$$

$$\boldsymbol{K}_5 = \begin{bmatrix} 10 & 0 & 0 \\ 0 & 10 & 0 \\ 0 & 0 & 1 \end{bmatrix} \tag{63}$$

$$\boldsymbol{q} = \begin{bmatrix} 0.1 & 0 & 0 \\ 0 & 0.01 & 0 \\ 0 & 0 & 0.01 \end{bmatrix} \tag{64}$$

The control signal for the crane force is increasing from 50s to 800s from 0 to maximum value, and decreasing from 1000s to 1750s from the maximum value to 0. If not explicitly pointed out, the maximum crane load is almost 500 tonnes as shown in Fig. 9. The parameters for the PI controller for the hydraulic motor in (11) are chosen as:

$$K_{hp} = 3.927 \tag{65}$$

$$K_{hi} = 0.393 \tag{66}$$

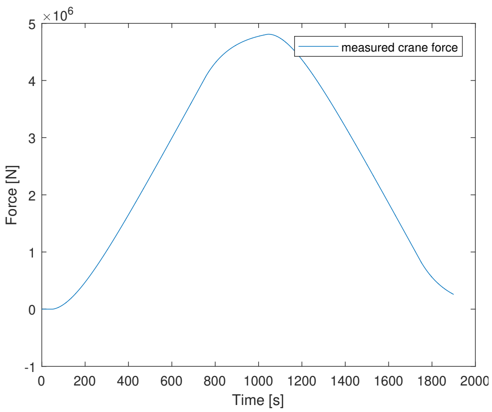

Fig. 9. Measured Force in Crane Wires

Fig. 9 shows the measured crane force in the crane wires with a maximum load of 500 tonnes. The direction of the force is not known in this case, and only the crane force is measured as a scalar.

Simulations are made under different simulated environments. The results of the estimation of horizontal crane force and position of the vessel are shown later in this section.

B. Simulation under Very Calm Sea State

In this part, simulation is made under very calm sea state, and the result is shown in Appendix I with 0.04% noise amplitude and 500t maximum load. With few environmental loads, the vessel position is very stable with a maximum offset of 5cm in surge, 2.5mm in sway and 6×10^{-5}rad in yaw. Crane force in surge direction is first increasing, then decreasing with little oscillation. The length of the crane wires is changing smoothly. East and yaw position of the vessel is oscillating within a small scale. The vessel is first moving to the front during loading and then moving to the back during offloading. The reason for this is that the pitch angle influences the Center of Origin of the vessel. A slight time delay in the observation of the vessel position and the crane force can be observed from the simulation. The time delay is approximately 0.48s in the north direction, 1.88s in east direction and 1.97s in the yaw direction.

C. Simulation under Sea State 2

A nominal simulation with the 500t maximum load under sea state two is made in this section. Results are shown in Appendix II. The maximum measurement noise in the crane force sensor is set to 0.04% of the real value. The maximum offset is around 0.12m in the north, 0.1m in the east, and 6×10^{-3}rad in yaw.

The position estimator gives the estimated low-frequency movement of the vessel which could be seen from Fig. 12. The estimation for the mooring stiffness is not shown because mooring stiffness is a virtual concept. In this simulation, the vessel is moving with a low-frequency oscillation which has a time-varying period. During the loading phase, when the crane wires are getting shorter, the mooring stiffness and the frequency of the motion are both increasing.

The estimated horizontal forces and moment are the product of the offsets and the mooring stiffness. They are compared with the real values in Fig. 13. The length of the crane wires shows that the vessel is first loading, then offloading the simulated load. The crane force in the horizontal direction is oscillating according to the real value in Fig. 13. The maximum crane forces and moment are around 6kN in surge, 8kN in sway and 900kNm in yaw. The oscillation of the crane load is a combination of low-frequency and high-frequency disturbances. Similar to the estimation for the position, the estimation for the force and moment is also focused on the low-frequency component of the force. The force in the surge direction has a changing mean value due to the change of the pitch angle. The high-frequency part in the horizontal crane force is filtered out in force and moment estimation.

D. Simulation under High Loading Rate

In this section, the model with the observer and PID controller is simulated with a maximum load of 1000t with double loading and offloading rates comparing to the nominal simulation. The results are shown in Appendix III. The results in Fig. 14 and Fig. 15 are similar comparing to the nominal simulation. The estimation for the horizontal load in surge direction, however, is less accurate when the actual force is high, i.e., around 1000 seconds where it has an error of approximately 1kN at the peak of the load.

E. Simulation under Low Load

In this simulation, the maximum load is set to 250t and results are shown in Appendix IV. Fig. 16 shows the estimation and measured value of the vessel position. Fig. 17 shows the estimation of the crane forces and moment. The oscillations of the crane forces and moment have smaller amplitudes comparing to the previous simulations. The vessel is less stable during the beginning of the loading process comparing to the previous simulations with a load of 500t and 1kt.

F. Simulation with High Measurement Noise

In this section, the measurement noise of the crane force is set to 2%, which is 50 times the original measurement noise. The results in Appendix V show that the noise does not have a significant influence on the performance of the proposed estimator.

G. Simulation with Uncertainty in the Observer Parameter

In this simulation, the mass matrix and damping matrix used to design the observer is set as 50% of the parameters used in the simulation model to test if the observer could handle design uncertainty of the vessel weight and damping. Results in Appendix V shows that with the given uncertainty, the observer could provide accurate estimations.

H. Simulation under Sea State 2 with the Influence of Current

In this simulation, the current velocity is set as 0.6m/s. The system is initialized for the bias observation at the start of the simulation. Results are shown in the appendix V. From the results, the observer can estimate the horizontal force and the position of the vessel. The influence of the current on the estimation of vessel position is minor. However, the estimations of the crane force in sway and the moment in yaw are less accurate.

I. Evaluation

To evaluate the overall performance of the observer under different circumstances, an index of integrated error $\bar{e}$ is used. Take the position estimation in surge direction as an example, the index is defined as:

$$\bar{e}_x = \frac{\int_{t_0}^{t_{end}} (\hat{\eta}_{surge} - \eta_{surge}) dt}{t_{end}} \tag{67}$$

Where t_0 is the starting time for the simulation, t_{end} is the ending time of the simulation.

The integrated errors of position and crane force estimations are shown in Table I and Table II.

TABLE I
INTEGRATED ERROR OF POSITION ESTIMATION

	$\bar{e}_x[m]$	$\bar{e}_y[m]$	$\bar{e}_\psi[rad]$
Sea State 0($\times 10^{-3}$)	0.1174	−0.0117	−0.0002
Sea State 2($\times 10^{-3}$)	−0.1079	−3.3436	0.2169
High Load($\times 10^{-3}$)	0.9829	−3.0466	−0.0527
Low Load($\times 10^{-3}$)	−0.7234	−3.8001	−0.0658
High Noise($\times 10^{-3}$)	−0.2719	−3.7896	−0.0663
Uncertainty($\times 10^{-3}$)	−0.5393	−7.6165	−0.1303
With Current($\times 10^{-2}$)	−3.4018	−2.5481	−0.0122

TABLE II
INTEGRATED ERROR OF FORCE ESTIMATION

	$\bar{e}_{fx}[N]$	$\bar{e}_{fy}[N]$	$\bar{e}_{f\psi}[Nm]$
Sea State 0($\times 10^{4}$)	0.0028	0.0001	−0.0072
Sea State 2($\times 10^{4}$)	0.0002	0.0306	−3.5198
High Load($\times 10^{4}$)	0.0229	0.0106	−1.2195
Low Load($\times 10^{4}$)	0.0175	−0.0009	0.0985
High Noise($\times 10^{4}$)	0.0284	0.0012	−0.1337
Uncertainty($\times 10^{4}$)	0.0280	−0.0104	1.1982
With Current($\times 10^{4}$)	0.0935	0.0202	−2.3182

According to Table I and Table II, the observer has the best performance under sea state 0 and the worst performance with uncertain parameters. The load estimation is less accurate in surge direction when the load and loading rate are increased.

V. CONCLUSION

In this work, we estimated the vessel position and the horizontal force induced by the crane wires during mooring mode of offshore heavy lift construction work. A new term 'mooring stiffness' was introduced to estimate the horizontal force. The position of the vessel and the horizontal crane force were estimated using a joint parameter-state observer which was based on the nonlinear passive observer. One advantage of the proposed observer is the reduction of measurements. The designed observer does not require the measured or estimated sway angle of the crane wires.

Besides, an integrated simulation model was made with vessel dynamics, hydraulic crane, environmental load, and thrusters to simulate the dynamic behavior of the crane vessel and to test the performance of the designed observer.

According to the simulation results, the estimations of the vessel position were accurate in various conditions. In particular, the estimation of the position in the north direction gave good results as shown in Table I. The largest offsets of the position estimation were noticed in the east direction and for high uncertainty of the modeled parameters. The estimations of the yaw position were also notably small. For the horizontal crane force, the observer could catch the low-frequency oscillation of the force but had difficulty following the high-frequency component of the horizontal load. As shown in Fig. 11, Fig. 13, Fig. 15, Fig. 17, Fig. 19, Fig. 21, and Fig. 23. The estimation of the crane force was able to obtain part of the high-frequency component of the horizontal load which was induced by the wave frequency. This happened for two reasons. Firstly, the impact of the measured high-frequency pitch and roll movement on the horizontal force is filtered. However, the crane tip has a significant movement due to the roll motion, which leads to high-frequency changes of sway force and yaw moment in the crane. Secondly, the estimations for vessel position and yaw angle work best at low frequency, and these estimated data sets are used to calculate the estimated crane force. So the force induced by the high-frequency movement of the vessel could not be observed in the crane force observer. However, this is not a problem in reality, because the thrusters of the vessel are not able to react fast enough to the high-frequency signal from the thrust allocator. Thus the filtering of high-frequency load and movement is good for further design and integration of the DP system.

The outcome of this work is useful for the estimation of the states of heavy lift vessels during offshore construction operations. The main novelty is an accurate estimation of the mean horizontal crane force stemming from the large mooring force in the offloading and loading mode. By obtaining these two estimates (i.e., the state estimates and the horizontal force estimate), the overall safety of offshore construction operations is improved as the DP operator is timely informed about the forces acting on the vessel. Moreover, the estimated data could be further used for controller design, such as feedforward or as the input switching signal to an adaptive controller that can adapt to different construction modes. The work presented in this paper is intended for further automation of the overall off-shore construction processes. In our future work, we intend to explore this approach and develop a complementary controller for highly automated offshore construction procedures.

Furthermore, this work can be developed regarding the assumptions made initially. As the proposed approach works under the assumption that the offset of the vessel is small, the estimation can only work in combination with a DP system which maintains the surge, sway, and yaw position of the vessel. We have further verified that when the yaw angle of the vessel is larger than 0.1 radian, the horizontal force estimation is not accurate anymore. Therefore, additional work could be done on the estimation of horizontal crane force when the yaw offset is larger than 0.1 radian. In this case, the dynamics of the crane vessel in the body-fixed frame should not be linearized anymore. Thus the nonlinear dynamics should be investigated, and a new estimation method could be developed to accommodate larger ship motions that are typical for higher sea states.

ACKNOWLEDGEMENT

We would like to thank Peter de Vos and Harsh Sapra for their help in the modeling of the propulsion systems, and would like to thank Xu Pengpeng for providing extra data about wave load on floating structures using finite volume method.

APPENDIX

A. Simulation under Sea State 0

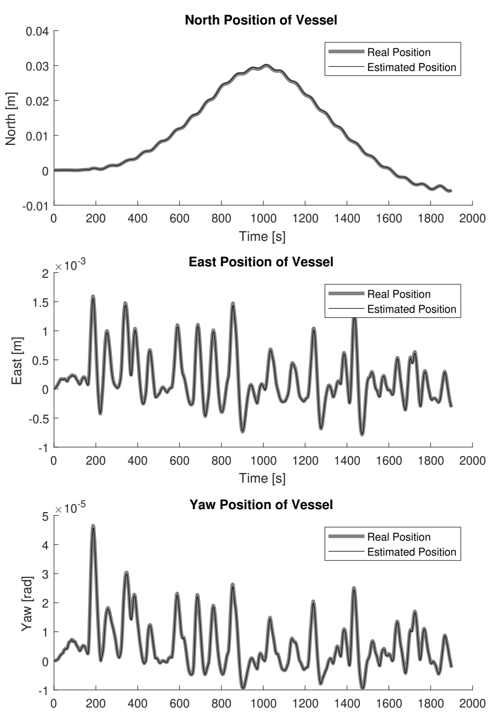

Fig. 10. Estimated Position and Real Position under Sea State 0

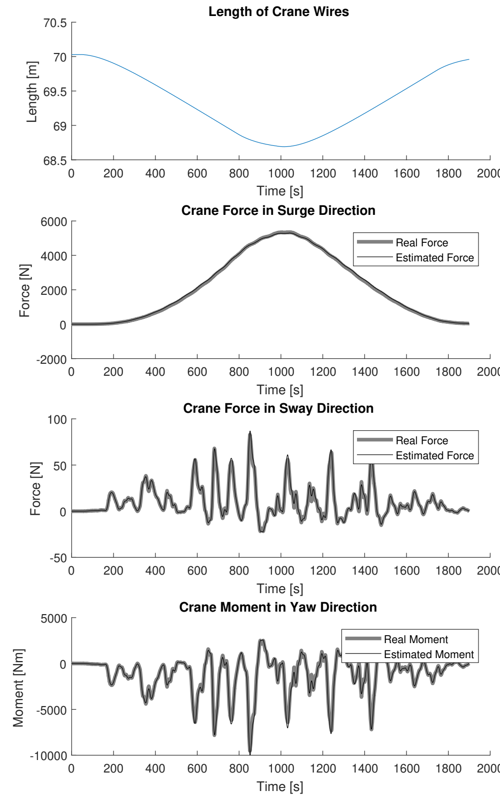

Fig. 11. Estimated Crane Force and Real Crane Force under Sea State 0

B. Simulation under Sea State 2

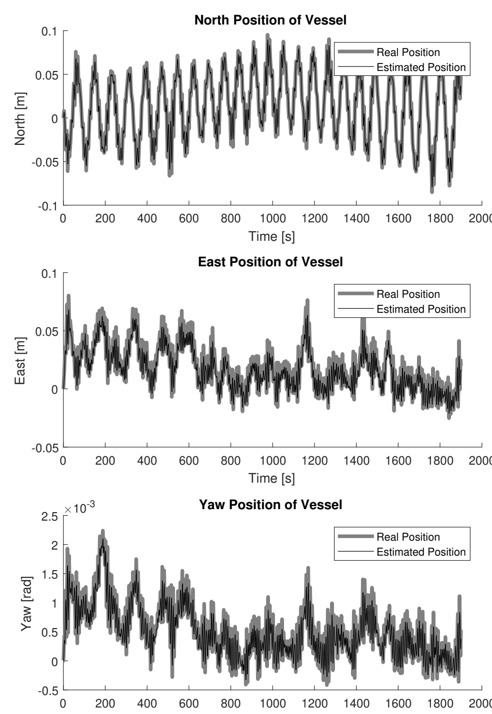

Fig. 12. Estimated Position and Real Position under Sea State 2

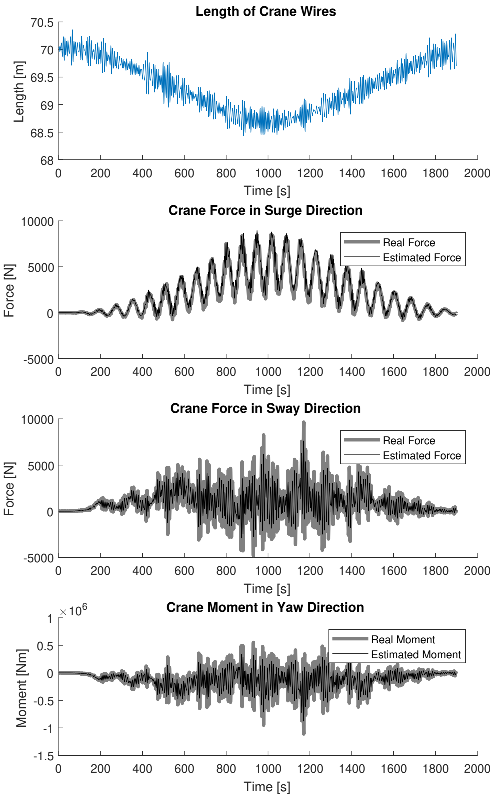

Fig. 13. Estimated Crane Force and Real Crane Force under Sea State 2

C. Simulation under High Load and High Loading Rate

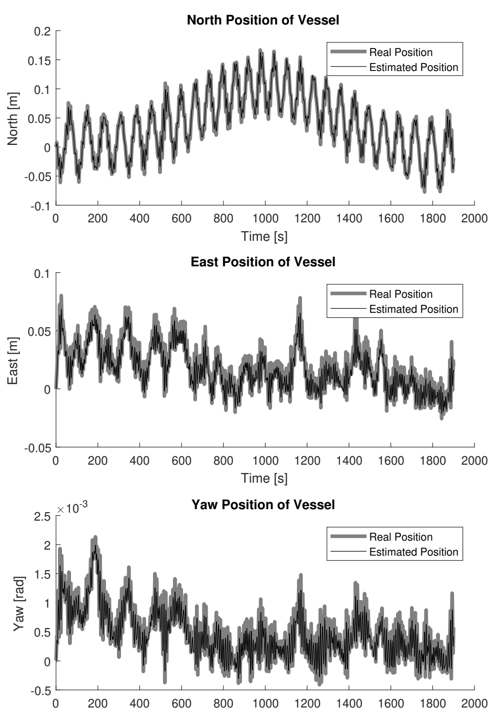

Fig. 14. Estimated Position and Real Position with Higher Load

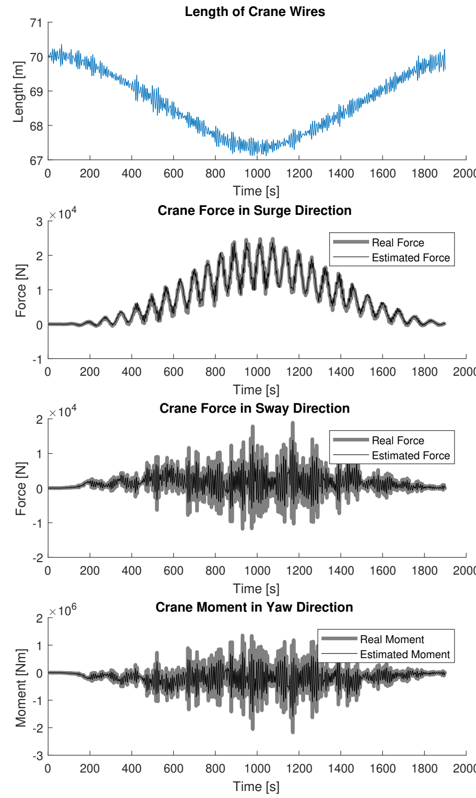

Fig. 15. Estimated Crane Force and Real Crane Force with Higher Load

D. Simulation under Low Load

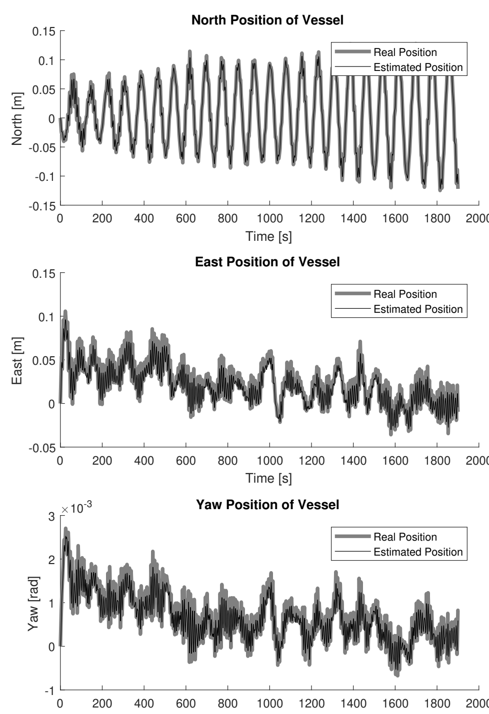

Fig. 16. Estimated Position and Real Position with Lower Load

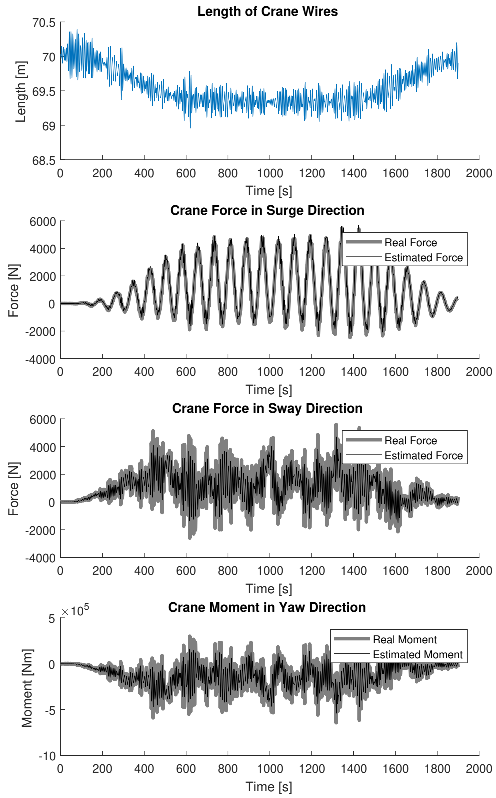

Fig. 17. Estimated Crane Force and Real Crane Force with Lower Load

E. Simulation with High Measurement Noise

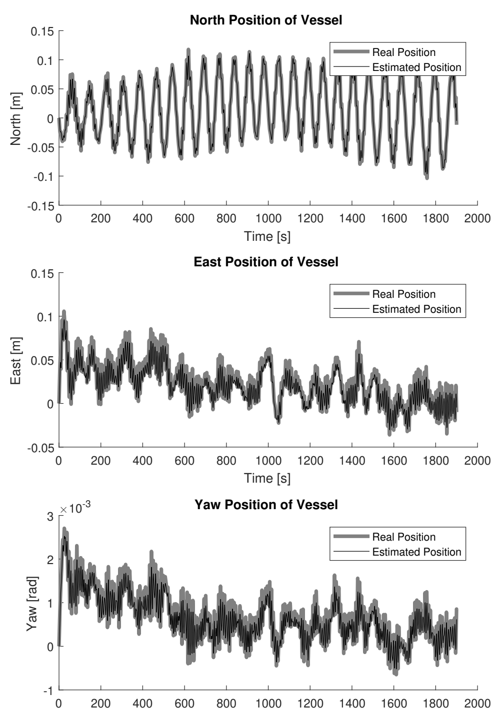

Fig. 18. Estimated Position and Real Position with High Noise

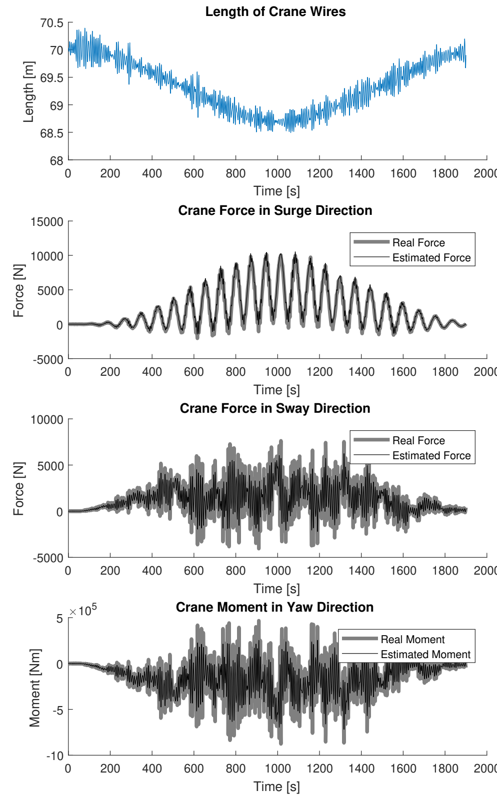

Fig. 19. Estimated Crane Force and Real Crane Force with High Noise

F. Simulation with Inaccurate Parameters

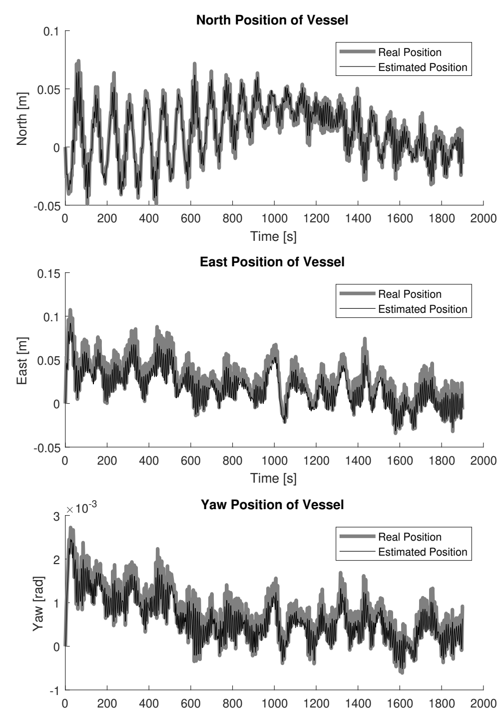

Fig. 20. Estimated Position and Real Position with Wrong Matrix

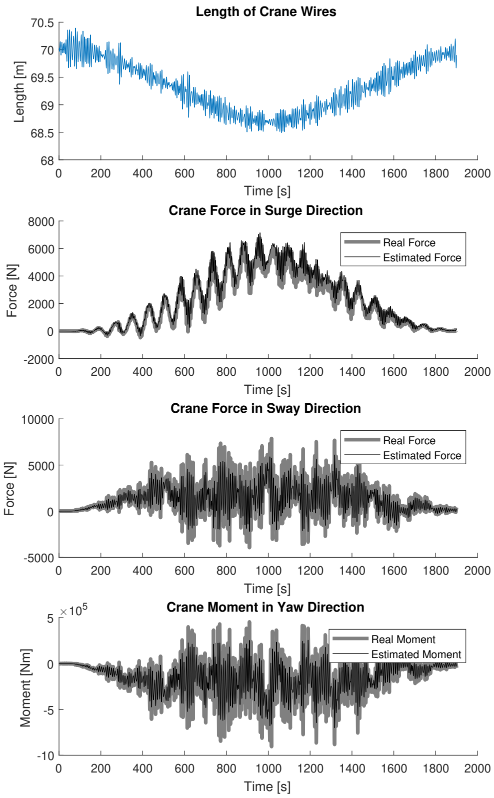

Fig. 21. Estimated Crane Force and Real Crane Force with Wrong Parameter Matrix

G. Simulation with Current

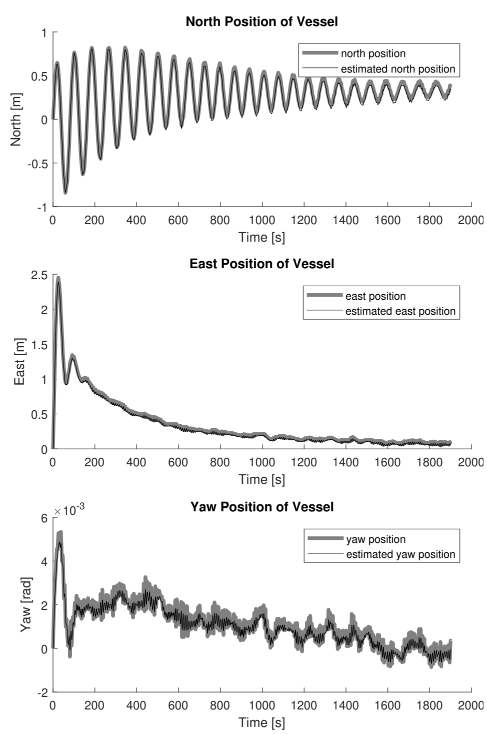

Fig. 22. Estimated Position and Real Position with Current of 0.6 m/s

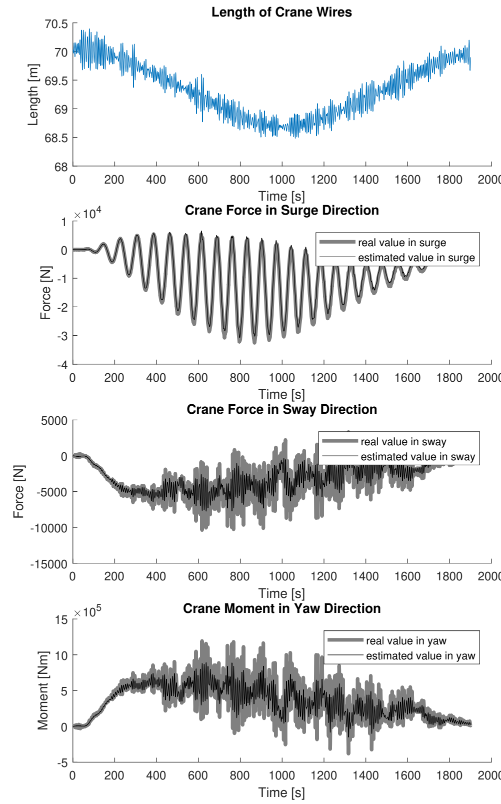

Fig. 23. Estimated Crane Force and Real Crane Force with Current of 0.6 m/s

REFERENCES

[1] Tan Y, Song Y, Liu X, Wang X, Cheng JCP. A BIM-based framework for lift planning in topsides disassembly of offshore oil and gas platforms. In: *Automation in Construction*. 2017;79:19-30. doi:10.1016/j.autcon.2017.02.008

[2] Li L, Gao Z, Moan T, Ormberg H. Analysis of lifting operation of a monopile for an offshore wind turbine considering vessel shielding effects. In: *Marine Structures*. 2014 Dec 1;39:287-314. doi:10.1016/j.marstruc.2014.07.009

[3] Osiński M, Maczyński A, Wojciech S. The influence of ship's motion in regular wave on dynamics of an offshore crane. In: *Archive of Mechanical Engineering*. 2004;51(2):131-63. ISSN: 2300-1895

[4] Hatecke H, Krüger S, Christiansen J, Vorhölter H. A fast sea-keeping simulation method for heavy-lift operations based on multi-body system dynamics. In: *ASME 2014 33rd International Conference on Ocean, Offshore and Arctic Engineering* 2014 Jun, San Francisco, USA. doi:10.1115/omae2014-23456

[5] Watters AJ, Moore DJ, McGill LS. Dynamics of offshore cranes. In: *Offshore Technology Conference*. 1980 May, Houston, Texas, USA. doi:10.4043/3792-ms

[6] Ellermann K, Kreuzer E. Markiewicz M. Nonlinear dynamics of floating cranes. In: *Nonlinear Dynamics*. 2002 Jan 1;27(2). doi: 10.1023/A:1014256405213

[7] Fang Y, Wang P, Sun N, et al. Dynamics analysis and nonlinear control of an offshore boom crane. In: *IEEE Transactions on Industrial Electronics*, 2014 Jan;61(1):414-427. doi:10.1109/tie.2013.2251731

[8] Flint J, Stephens R. Dynamic positioning for heavy lift applications. In: *Dynamic Positioning Conference*, 2008, Huston, Texas, USA. https://dynamic-positioning.com/proceedings/dp2008/newapps_flint.pdf

[9] Vorhölter H, Hatecke H, Feder DF. Design study of floating crane vessels for lifting operations in the offshore wind industry. In: *Proceedings of '15 International Marine Design Conference*. 2015 May:1-13. http://www.ssi.tu-harburg.de/doc/webseiten_dokumente/ssi/veroeffentlichungen/IMDC_2015_Vorhoelter_Hatecke.pdf

[10] Raja Ismail RMT, Nguyen D, Ha QP. Modelling and robust trajectory following for offshore container crane systems. In: *Automation in Construction*. 2015;59:179-187. doi:10.1016/j.autcon.2015.05.003

[11] Fang Y, Dixon WE, Dawson DM, et al. Nonlinear coupling control laws for an underactuated overhead crane system. In: *IEEE/ASME Transactions on Mechatronics*, 2003 Sep;8(3):418-23. doi:10.1109/tmech.2003.816822

[12] Ngo QH, Hong KS. Sliding-mode antisway control of an offshore container crane. In: *IEEE/ASME Transactions on Mechatronics*. 2012 Apr;17(2):201-9. doi:10.1109/tmech.2010.2093907

[13] Sun N, Fang Y, Chen H and He B. Adaptive nonlinear crane control with load hoisting/lowering and unknown parameters: design and experiments. In: *IEEE/ASME Transactions on Mechatronics*, 2015 Oct;20(5):2107-2119. doi:10.1109/tmech.2014.2364308

[14] Huang J, Xie X and Liang Z. Control of bridge cranes with distributed-mass payload dynamics. In: *IEEE/ASME Transactions on Mechatronics*, 2015 Feb;20(1):481-486. doi:10.1109/tmech.2014.2311825

[15] Sun N, Fang Y, Chen H, Wu Y, et al. Nonlinear antiswing control of offshore cranes with unknown parameters and persistent ship-Induced perturbations: theoretical design and hardware experiments. In: *IEEE Transactions on Industrial Electronics*, 2018 Mar;65(3):2629-2641. doi:10.1109/tie.2017.2767523

[16] Küchler S, Mahl T, Neupert J, Schneider K, Sawodny O. Active control for an offshore crane using prediction of the vessel's motion. In: *IEEE/ASME Transactions on Mechatronics*. 2011 Apr;16(2):297-309. doi:10.1109/tmech.2010.2041933

[17] Skaare B, Egeland O. Parallel force/position crane control in marine operations. In: *IEEE Journal of Oceanic Engineering*. 2006 Jul;31(3):599-613. doi:10.1109/joe.2006.880394

[18] Messineo S, Serrani A. Offshore crane control based on adaptive external models. In: *Automatica*. 2009 Nov 1;45(11):2546-56. doi:10.1109/acc.2008.4586866

[19] Bakker FC. *A conceptual solution to instable dynamic positioning during offshore heavy lift operations using computer simulation techniques*. Msc thesis, TU Delft, NL, 2015. https://repository.tudelft.nl/islandora/object/uuid:25994611-b8c1-442a-85be-d6c18f02bdba?collection=education

[20] Ye J. *Dynamic positioning during heavy lift operations: using fuzzy control techniques, nonlinear observer and H-infinity method separately to obtain stable DP systems for heavy lift operations*. Msc thesis, TU Delft, NL, 2016. https://repository.tudelft.nl/islandora/object/uuid:b62c6893-800f-4ee5-b52a-d4eff7c69201?collection=education

[21] Zhou L, Moan T, Riska K, Su B. Heading control for turret-moored vessel in level ice based on Kalman filter with thrust allocation. In: *Journal of Marine Science and Technology*, 2013 Dec 1;18(4):460-70. doi:10.1007/s00773-013-0220-7

[22] Nord TS, Lourens EM, Øiseth O, Metrikine A. Model-based force and state estimation in experimental ice-induced vibrations by means of Kalman filtering. In: *Cold Regions Science and Technology*, 2015 Mar 1;111:13-26. doi:10.1016/j.coldregions.2014.12.003

[23] Nord TS. *Force and response estimation on bottom-founded structures prone to ice-induced vibrations*. PhD Thesis, NTNU, Norway, 2015. https://core.ac.uk/download/pdf/154668139.pdf

[24] Ohtomo S, Murakami T. Estimation method for sway angle of payload with reaction force observer. In: *In Advanced Motion Control (AMC), 2014 IEEE 13th International Workshop*, 2014 Mar 14:581-585. doi:10.1109/amc.2014.6823346

[25] Fossen TI and Perez T. Marine Systems Simulator (MSS). 2004. http://www.marinecontrol.org.

[26] Fossen TI. *Handbook of marine craft hydrodynamics and motion control*. John Wiley & Sons; 2011 May 23. doi:10.1002/9781119994138

[27] Brater EF, King HW, Lindell JE and Wei CY. *Handbook of hydraulics for the solution of hydraulic engineering problems (Vol. 7)*. New York: McGraw-Hill; 1996. ISBN: 9780070072473

[28] Geertsma RD, Negenborn RR, Visser K, Loonstijn MA, & Hopman JJ. Pitch control for ships with diesel mechanical and hybrid propulsion: Modelling, validation and performance quantification. In: *Applied Energy*, 2017, 206: 1609–1631. doi:10.1016/j.apenergy.2017.09.103

[29] Godjevac M, Drijver M. Performance evaluation of an inland pusher. In: *Transport of Water versus Transport over Water*, 2015: 389-411. doi:10.1007/978-3-319-16133-4_20

[30] Fossen TI, Strand JP. Passive nonlinear observer design for ships using Lyapunov methods: full-scale experiments with a supply vessel. In: *Automatica*. 1999 Jan 1;35(1):3-16. doi:10.1016/s0005-1098(98)00121-6